Applied Catalysis B: Environmental 315 (2022) 121519

Contents lists available at ScienceDirect

Applied Catalysis B: Environmental

journal homepage: www.elsevier.com/locate/apcatb

Sulfate radical anion: Laser flash photolysis study and application in water disinfection and decontamination

Ilaria Berruti [a], María Inmaculada Polo-López [a,b,*], Isabel Oller [a,b], Jenny Flores [c], M. Luisa Marin [c,**], Francisco Bosca [c]

[a] CIEMAT-PSA, Carretera de Senés Km 4, Tabernas, Almería 04200, Spain
[b] CIESOL, Joint Centre of the University of Almería-CIEMAT, Almería 04120, Spain
[c] Instituto de Tecnología Química, Universitat Politècnica de València-Consejo Superior de Investigaciones Científicas, Avda. de los Naranjos s/n, Valencia E-46022, Spain

ARTICLE INFO

Keywords:
Bacteria
CECs
Quenching rate constants
Time-resolved kinetics
UV-C/Persulfate

ABSTRACT

Sulfate radicals ($SO_4^{\bullet-}$) reactivity against gram-negative (*E. coli*) and gram-positive (*E. faecalis*) bacteria and Contaminants of Emerging Concern (CECs) (Diclofenac-DCF, Sulfamethoxazole-SMX and Trimethoprim-TMP) was investigated through laser flash photolysis (LFP) technique. Analysis of the lifetime of $SO_4^{\bullet-}$ in presence of cell-wall compounds of bacteria and CECs allowed determining reactivity of $SO_4^{\bullet-}$ towards these compounds. Results showed that $SO_4^{\bullet-}$ reacts with common cell-wall components through H-abstraction mechanism ($k_{SO4\bullet-} < 10^8$ $M^{-1}s^{-1}$). By contrast, $k_{SO4\bullet-} > 10^9$ $M^{-1}s^{-1}$ were found using aromatic amino acids (AAA) only present in Porins of the gram-negative outer-membrane. The intermediates detected from the reaction of $SO_4^{\bullet-}$ with the AAA confirmed the involvement of electron transfer processes. Moreover, $k_{SO4\bullet-}$ values determined for DCF, TMP and SMX also agreed with an electron transfer mechanism. Interestingly, bacteria and CECs removal at pilot plant scale by UV-C/$SO_4^{\bullet-}$ is in accordance with the $k_{SO4\bullet-}$ obtained using the LFP: *E. coli* > *E. faecalis* and DCF > TMP ≅ SMX.

1. Introduction

Sulfate Radical-based Advanced Oxidation Processes (SR-AOPs) are gaining attention as attractive and promising treatments for simultaneous degradation of Contaminants of Emerging Concern (CECs) and for inactivation of waterborne pathogens in different water matrices, including surface waters and wastewaters (industrial and domestic) [1,2]. The key of SR-AOPs is the generation of highly reactive species (mainly sulfate radical anion $SO_4^{\bullet-}$) in solution through the activation of persulfate (PS), with different methods including heat, UV-C light, radiolysis, and transition metals [3]. The homolytic rupture of the peroxy bond in PS leads to the production of two moles of $SO_4^{\bullet-}$ per mol of $S_2O_8^{2-}$ reacted. The formed $SO_4^{\bullet-}$ is a single electron oxidant with high redox potential (E_{red} ($SO_4^{\bullet-}/SO_4^{2-}$) = 2.43 V *vs* Normal Hydrogen Electrode (NHE)), that exhibits higher selectivity and longer half-life than hydroxyl radical ($HO^{\bullet}$) [4,5].

Different mechanisms have been postulated to account for the first step of radical oxidation of organic compounds in the presence of $SO_4^{\bullet-}$ [5–7]. Thus, initially, single electron transfer reactions can be postulated for electron-rich molecules such as aromatic compounds, and in fact they show bimolecular rate constants ($k_{SO4\bullet-}$) in the range 10^8–10^9 M^{-1} s^{-1}; whereas, H-abstraction reactions are mainly generated from aliphatic compounds and they display $k_{SO4\bullet-}$ in the range 10^5–10^7 M^{-1} s^{-1} [5]. Recently, it has been evidenced the possibility that addition of $SO_4^{\bullet-}$ to a double bond of an organic molecule could take place, and $k_{SO4\bullet-}$ values in the range of 10^5–10^9 M^{-1} s^{-1} have been proposed for this alternative, in the order of the values associated with electron transfer and H-abstraction [5,6]. This third option is analogous to the reported addition of $HO^{\bullet}$ to the double bond of aromatic compounds [8]. Moreover, when the concentration of the target organic compounds decreases, $SO_4^{\bullet-}$ would result into the formation of other Reactive Oxygen species (ROS) (mainly $HO^{\bullet}$) that eventually could also participate in the photodegradation.

Furthermore, studies about water disinfection by $SO_4^{\bullet-}$ have

* Correspondence to: Plataforma Solar de Almería-CIEMAT, P.O. Box 22, Tabernas, Almería 04200, Spain.
** Corresponding author.
E-mail addresses: iberruti@psa.es (I. Berruti), mpolo@psa.es (M. Inmaculada Polo-López), ioller@psa.es (I. Oller), jenfloga@doctor.upv.es (J. Flores), marmarin@qim.upv.es (M. Luisa Marin), fbosca@itq.upv.es (F. Bosca).

https://doi.org/10.1016/j.apcatb.2022.121519
Received 8 March 2022; Received in revised form 11 May 2022; Accepted 13 May 2022
Available online 17 May 2022

evidenced the ability of this intermediate to inactivate bacteria and fungi [9–12]. However, the disinfection mechanism is not well understood. In fact, in one of them it has been described that UV-A light and peroxymonosulfate (PMS) produced inactivation of three different bacteria, with gram-negative (*Escherichia coli*) reaching the fastest and highest yield, followed by non-sporulated gram-positive (*Staphylococcus aureus*) and sporulated gram-positive (*Bacillus mycoides*) [10]. In a different study, using zero valent iron (ZVI) and PS for generating $SO_4^{\bullet-}$, a faster inactivation of gram-positive bacteria (*Enterococcus faecalis*) than gram-negative one (*E. coli*) was observed [9].

Thereby, a deeper knowledge on the reactivity of $SO_4^{\bullet-}$ with contaminants, and also with the components of bacteria membrane is crucial to understand the degradation of pollutants, as well as, the processes involved in the bacteria inactivation. In this context, among the time-resolved techniques, laser flash photolysis (LFP) has demonstrated to be a valuable methodology to determine reaction rate constants and to investigate mechanisms of reaction. It is based on the detection and kinetic analysis of short-lived excited states and intermediates, usually in the microsecond time-scale [13]. Photolysis of PS with excitation wavelength $\lambda_{exc} < 300$ nm is a clean source of $SO_4^{\bullet-}$, with high quantum yield independent from pH range. In this scenario, LFP technique allows to easily detect $SO_4^{\bullet-}$, while other radicals (such as $HO^{\bullet}$), that could be formed at lower concentration and with lower extinction coefficient, can be discarded as interfering elements in the analysis. Subsequently, LFP studies have proven to yield information on absolute rate constants ($k_{SO4\bullet-}$) with different organic compounds, including pharmaceuticals, pesticides, additives, dyes, surfactants and artificial sweeteners [5,14–17]. Interestingly, LFP has never been employed to investigate the mechanisms involved in microbial inactivation by SR-AOP.

The present study provides a mechanistic understanding on water disinfection and decontamination by SR-AOPs. Thereby, LFP experiments performed upon generation of $SO_4^{\bullet-}$ by laser irradiation of PS with UV-C wavelengths allowed determining the reactivity of $SO_4^{\bullet-}$ with different chemicals. In the case of bacteria, specific constituents of gram-positive and gram-negative bacteria cell walls were investigated. The results were compared to those obtained for aromatic amino acids (AAA) contained in porins, proteins only present in the structure of the gram-negative outer-membrane. Besides, the mechanism operating on the abatement of three CECs such as Diclofenac (DCF), Sulfamethoxazole (SMX) and Trimethoprim (TMP), compounds commonly present in different contaminated water sources, has also been elucidated. Moreover, this study provided the experimental assessment of different bacteria (*E. coli* K12 and *E. faecalis*) inactivation and CECs degradation in water by $SO_4^{\bullet-}$, using a PS/UV-C system (at pilot scale).

2. Materials and methods

2.1. Chemical reagents

Sodium persulfate (PS) ($Na_2S_2O_8$), isopropanol, methanol and NaN_3 were purchase from Sigma Aldrich and used as received. Cell-wall components: *N*-acetylmuramic acid; *N*-acetyl-*L*-alanine; 2,6-Diaminopimelic acid; *N*-acetyl-*D*-glucosamine; *N*-acetyl-*L*-lysine and *N*-acetyl-*D,L*-glutamic acid (chemical structures shown in Fig. S1, Supplementary material) were obtained from Fluorochem Limited and used as received. Tryptophan methyl ester hydrochlroride (Trp), Tyrosine (Tyr) and Phenylalanine (Phe), Diclofenac (DCF), Sulfamethoxazole (SMX) and Trimethoprim (TMP) were purchased from Sigma-Aldrich with high purity grade (> 99%) and used as received.

2.2. Laser flash photolysis (LFP) experiments

A pulsed ND:YAG SL404G-10 Spectron Laser System was employed to carry out the LFP experiments. The generation of $SO_4^{\bullet-}$ was produced from the photolysis of PS using a laser pulse at 266 nm, as excitation wavelength, and a pulse energy of 30 mJ. Quartz cells of 1 cm optical path-length with a total volume of 3 mL were employed for all measurements. An appropriate volume of stock solution of PS, to reach an initial concentration of 0.1 M, was mixed with a correct amount of different Quenchers (Q), *i.e.*, the chemical reagents evaluated in this study, just before each measurement to obtain the desired concentrations.

The lifetime of the $SO_4^{\bullet-}$ was recorded upon addition of increasing concentrations of each Q, and the bimolecular rate constants $k_{SO4\bullet-}$, (M^{-1} s^{-1}) were determined applying the Stern-Volmer equation (Eq. 1) and by using a linear regression of the decay rate of $SO_4^{\bullet-}$ *versus* Q concentration (Stern-Volmer plot). The slope of the straight line yielded the bimolecular rate constant k_Q (M^{-1} s^{-1}):

$$\frac{1}{\tau} = \frac{1}{\tau_0} + k_Q \bullet [Q] \quad (1)$$

where, τ = Lifetime of $SO_4^{\bullet-}$ recorded at a given concentrations of quencher Q (s); τ_0 = Lifetime of $SO_4^{\bullet-}$ recorded in the absence of quencher (s); [Q]= Quencher concentration (M); k_Q = bimolecular reaction rate constant $k_{SO4\bullet-,Q}$ (M^{-1} s^{-1}).

2.3. Water disinfection and decontamination by UV-C experiments

2.3.1. UV-C pilot plant and experimental procedure

UV-C water treatments were performed at pilot plant scale. It consists of three low pressure lamps (254 nm peak wavelengths, 230 W) protected by quartz tubes and axially located in a stainless steel cylindrical photoreactor [18]. In this study, experiments were performed with one UV-C lamp with a flow-rate of 36 L/min in batch mode. Total volume of water was 80 L, corresponding to an illuminated volume of 6.21 L per lamp module and an illuminated area of 0.338 m^2. A constant irradiance value 104 ± 3 W/m^2 was recorded during the treatment time (30 min).

Bacteria and CECs were treated separately and a correct amount of stock solution was added to the reactor previously filled with demineralized water to obtain an initial concentration of bacteria equal to 10^6 CFU/mL and of CECs of 100 μg/L each one. The system was homogenized in the dark and a control sample was taken (to probe the right initial concentration of bacteria and of contaminants). Then the desired concentration of PS (initial concentration ranged from 1 to 5 × 10^{-4} M) was spiked in the reactor and lamp switched on, immediately starting the irradiation experiment. PS concentration was chosen based on previous work [18]. Water samples were taken at regular time intervals for bacterial enumeration and CECs quantification. Two replicated experiments were carried out for each operation condition and all data are plotted in graphs as the average value with the standard deviation as error bar.

Water temperature (by a thermometer (Checktemp, Hanna, Spain)), pH (by a pH-meter (110-K, Horiba Laqua act)) and PS concentration, by using an iodometric method described elsewhere, were also regularly monitored [18]. Iodometric method briefly consists of the mixing of 3.5 mL of 71.4 g/L KI solution and 0.5 mL of 50 g/L $NaHCO_3$ solution with 1 mL of water sample, allowed to react for 15 min, and then the absorbance at 352 nm was measured with a UV–vis spectrophotometer (Evolution 220, Thermo Scientific). Water T remained constant during the treatment (26 ± 1) ºC, initial pH value (ranged 6.5–5.5) showed a slight decrease (1–2 pH values) after the treatment, not affecting in any case the inactivation of bacteria, the CEC degradation results or acting as promoter of PS activation, because T higher than 50 °C is necessary to generate $SO_4^{\bullet-}$ [19]. PS concentration measured during experiments is shown in Fig. S2 (Supplementary material).

2.3.2. Bacterial enumeration and quantification

E. coli K-12 (CECT 4624) and *E. faecalis* (CECT 5143) were provided by Spanish Culture Collection (CECT) and they were cultured in Luria-Bertani Broth (Merck KGaA®, Darmstadt, Germany). A suspension

with a concentration ~10^9 CFU/mL was obtained after incubation in a rotary shaking incubator at 37 °C and 100 rpm for 20 h. It was centrifuged for 15 min at 3000 rpm and bacterial pellets were re-suspended in phosphate-buffered saline (PBS) solution and directly diluted in the sample to obtain an initial concentration of 10^6 CFU/mL. Water samples were serial diluted in PBS and enumerated using the standard plate counting method. 50 μL of diluted samples and 500 μL of samples (when a significant bacterial concentration reduction was expected) were spread on ChromoCult® Coliform Agar (Merck KGaA®, Darmstadt, Germany), and Slanetz Bartley agar (Scharlau, Spain) and incubated 24 h for *E. coli* (at 37 °C) and 48 h for *E. faecalis* (at 37 °C), respectively. Detection limit (DL) was 2 CFU/mL [20].

2.3.3. CECs preparation and quantification

SMX, DCF and TMP stock solutions (at concentration of 8 mg/L) were prepared by dissolving the proper amount in MilliQ water and stored for further use (during 5 days). Concentration of each CEC along the experimental time were monitored by UPLC/UV (Agilent Technologies, Series 1260), using a C-18 analytical column (Poroshell 120 EC -C18 3.0 ×50 mm 2.7 μm), 100 μL of injection volume and flow rate of 1 mL/min. Initial conditions were 95% water with 25 mM formic acid (mobile phase A) and 5% acetonitrile (mobile phase B). A linear gradient progressed from 5% of B to 90% in 12 min and then at 100% for 1 min. The re-equilibration time was 3 min. DCF, SMX and TMP were detected at 285, 267, 273 nm and 7.6, 3.5 and 2.5 min of retention time, respectively. A 4.5 mL water sample was filtered through a 0.2 μm syringe-driven filter (Merck Millipore filter Hydrophobic (PTFE)) and washed with 0.5 mL of acetonitrile to remove any adsorbed organic compounds before analysis by UPLC/UV. Limit of quantification (LOQ) for DCF, SMX and TMP was 8, 8 and 20 μg/L, respectively [20].

2.3.4. Bacterial removal profiles and kinetic analysis of CECs

A microbial kinetic analysis was performed by fitting the experimental data following a double log-linear kinetics (Eq. 2), with a first stage very fast (k_1) and a second phase of attenuated inactivation (k_2) ($k_1 > k_2$) [21].

$$Log\left(\frac{N_t}{N_0}\right) = -k_1.\lambda t \quad t = (0, \quad t_1);\ Log\left(\frac{N_t}{N_0}\right) = -k_2.\lambda t \quad t = (t_1, \quad t_2) \tag{2}$$

where N_0 and N_t correspond to the bacterial concentration (expressed in CFU/mL) at time 0 min and at any specific time, respectively, k_1 is the first stage kinetic constant while k_2 the second one (k, min^{-1}).

Contaminants degradation obeyed pseudo-first order kinetics (Eqs. 3 and 4):

$$\frac{dC}{dt} = \quad -kC \tag{3}$$

$$ln\left(\frac{C_t}{C_o}\right) = -kt \tag{4}$$

where C_0 and C_t are initial and sampling time concentrations of CECs, respectively. The slope of the regression line, k (min^{-1}) is the pseudo-first order rate constant.

Table S1 (Supplementary Material) shows the analysis of the experimental data with the corresponding kinetic constants (k, min^{-1}) and the correlation coefficient (R^2) for each bacterium and CEC investigated at pilot plant scale.

2.3.5. Radical scavenger experiments

Scavenger experiments were carried out under UV-C radiation (UV lamp Trojan UV-01, 14 W) by using a pilot plant that allowed to treated lower volume of water (10 L), with a flow of 3.3 L/min in batch mode and an irradiance value of 28 W/m^2. Target contaminants were spiked at an initial concentration of 1 mg/L (chosen to obtain lower degradation rate and to observe a clearer quenching effect), while tert-butanol (TBA), a well-known scavenger agents of $HO^{\bullet}$, was used 1000-times more concentrated (at concentration of 4 ×10^{-3} M).

3. Results and discussion

3.1. Radical sulfate ($SO_4^{\bullet-}$) generation and reaction mechanisms

Generation of $SO_4^{\bullet-}$ was produced *in situ* upon LFP irradiation (at 266 nm) of an aqueous solution of PS (0.1 M) (Fig. S3 for the UV-Vis absorption spectrum) according to reaction (R1):

$$S_2O_8^{2-} + h\nu \rightarrow 2\ SO_4^{\bullet-} \tag{R1}$$

The transient absorption spectrum of $SO_4^{\bullet-}$ was recorded between 700 and 300 nm in the absence and presence of air (Fig. S4a and b). They showed an intense maximum absorption at 450 nm and a second less intense maximum at 320 nm, in agreement with previous data in literature [22]. Besides, decay traces of $SO_4^{\bullet-}$ in the absence and presence of air are shown in Fig. S4c; the two traces are superimposable, which acted as a piece of evidence of the insignificant reactivity of $SO_4^{\bullet-}$ with O_2. Therefore, from now on the transient decay of $SO_4^{\bullet-}$ was monitored at 450 nm under air, permitting to determine a decrease of the transient species with a pseudo first order constant of 1.3 × 10^5 s^{-1} and a lifetime τ_0 of *ca.* 6–8 μs under our experimental conditions, in agreement with literature data [17,23].

With this fitted operational conditions, reactivity of $SO_4^{\bullet-}$ with any organic compound can be determined analysing decay traces of $SO_4^{\bullet-}$ after the addition of different concentrations of the compound under study. The obtained $k_{SO4\bullet-}$ are crucial for understanding the oxidation processes involved in the degradation. In fact, the $k_{SO4\bullet-}$ values for the two main oxidation mechanisms, *i.e.*, H-abstraction or electron transfer process, were preliminary determined by LFP by using two alcohols (isopropanol and methanol) and NaN_3, respectively [5,24,25]. Therefore, these obtained kinetic rate constants values could be taken as the typical ranges of reactivity of $SO_4^{\bullet-}$ associated to each mechanism. In this context, although it has been suggested in a theoretical study that H-abstraction, electron transfer process and the addition of $SO_4^{\bullet-}$ to aromatic rings of the compounds can participate in the oxidation of organic compounds by $SO_4^{\bullet-}$ [8], the experimentally obtained $k_{SO4\bullet-}$ will only discriminate between H-abstraction and (apparent) electron transfer mechanisms.

The H-abstraction reaction between $SO_4^{\bullet-}$ and the C-H moiety was investigated using isopropanol (R2) and methanol (R3):

$$SO_4^{\bullet-} + C_3H_7OH \rightarrow SO_4^{2-} + (CH_3)_2\,{}^{\bullet}COH + H^+ \tag{R2}$$

$$SO_4^{\bullet-} + CH_3OH \rightarrow SO_4^{2-} + {}^{\bullet}CH_2OH + H^+ \tag{R3}$$

Thus, the decay of $SO_4^{\bullet-}$ at 450 nm was monitored in the presence of increasing amounts of isopropanol, in the range of 5 × 10^{-4} – 1 × 10^{-2} M (Fig. 1a), and the corresponding Stern-Volmer plot is shown in Fig. 1b. From the slope of the Stern-Volmer analysis a value of (6.77 ± 0.08) × 10^7 $M^{-1}s^{-1}$ for the bimolecular rate constant was determined. When methanol was tested as the H-donor species (Fig. 1c), the bimolecular rate constant value was lower, (1.01 ± 0.08) × 10^7 $M^{-1}s^{-1}$ (Fig. 1d), as expected from a primary alcohol compared to the secondary one [24]. Therefore, $k_{SO4\bullet-}$ values in the range 10^7 $M^{-1}s^{-1}$ can be associated to H-abstraction mechanism.

To investigate the electron transfer mechanism, NaN_3 was selected as an appropriate electron donor, since it has a redox potential of only 1.35 ± 0.02 V (*vs* NHE) [25]. Hence, the behaviour of $SO_4^{\bullet-}$ at 450 nm in the presence of increasing concentrations of NaN_3 (range of 1.65 ×10^{-4} −1.33 ×10^{-3} M), revealed an efficient decrease in the lifetime of the former (Fig. 1e). The determined bimolecular rate constant value from the Stern-Volmer analysis (Fig. 1f) was (1.22 ± 0.03) × 10^9 $M^{-1}s^{-1}$, in good agreement with data reported in the literature [26]. This value can

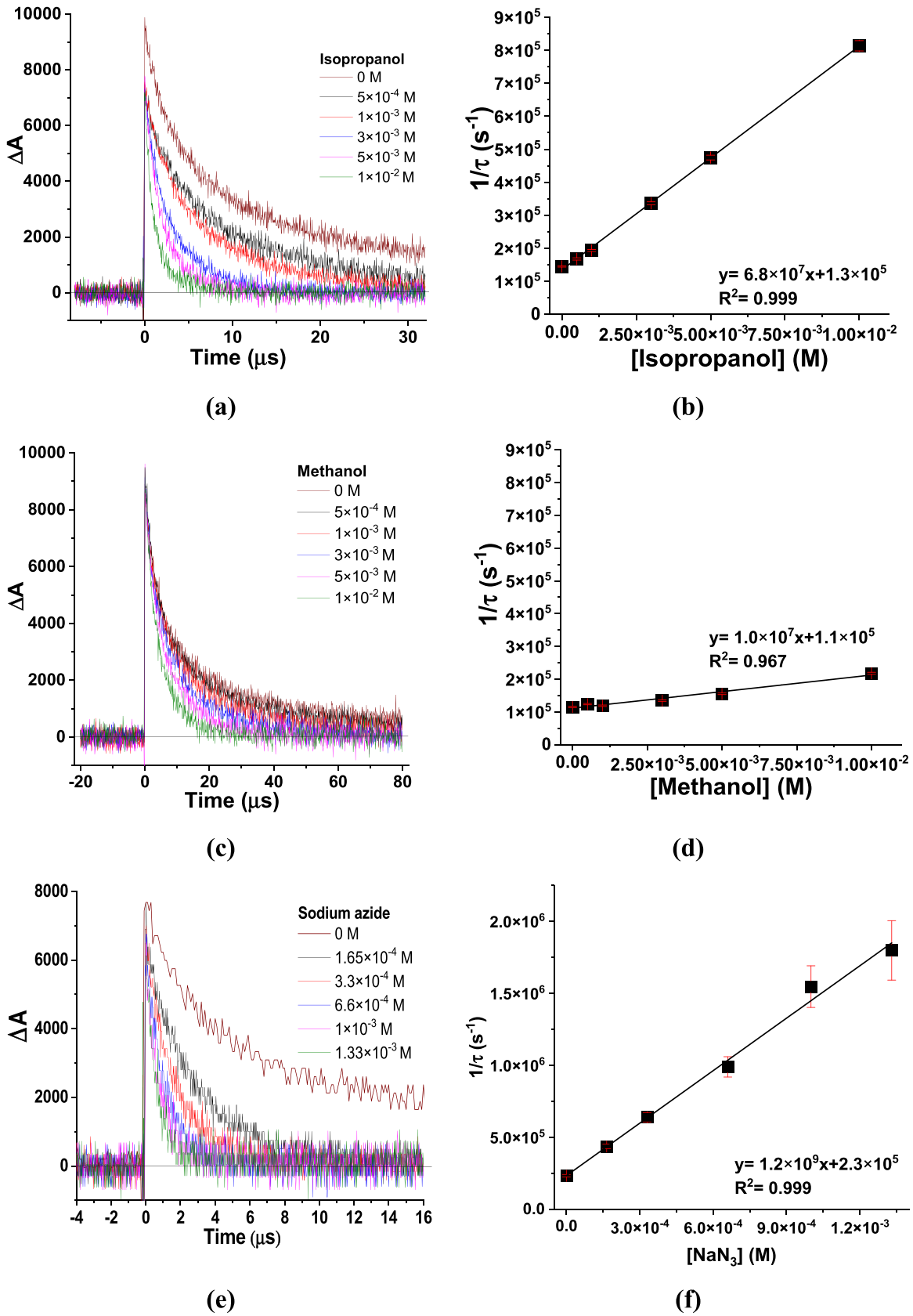

Fig. 1. Decay of $SO_4^{\bullet-}$, monitored at 450 nm, obtained from laser flash excitation (λ_{exc} = 266 nm) of aerated aqueous solutions of PS (0.1 M), in the presence of increasing concentrations of isopropanol (a); methanol (c) or NaN_3 (e); Corresponding Stern-Volmer plots (b; d and f).

clearly be associated to an electron transfer process because the reaction between $SO_4^{\bullet-}$ and electron donor molecules, if occurs, usually exhibits $k_{SO4\bullet-}$ values in the range 10^8-10^9 $M^{-1}s^{-1}$ [5].

Besides, it should be noted that the electron transfer mechanism is almost two orders of magnitude faster in comparison with the H-abstraction process, which is therefore directly correlated with a faster degradation.

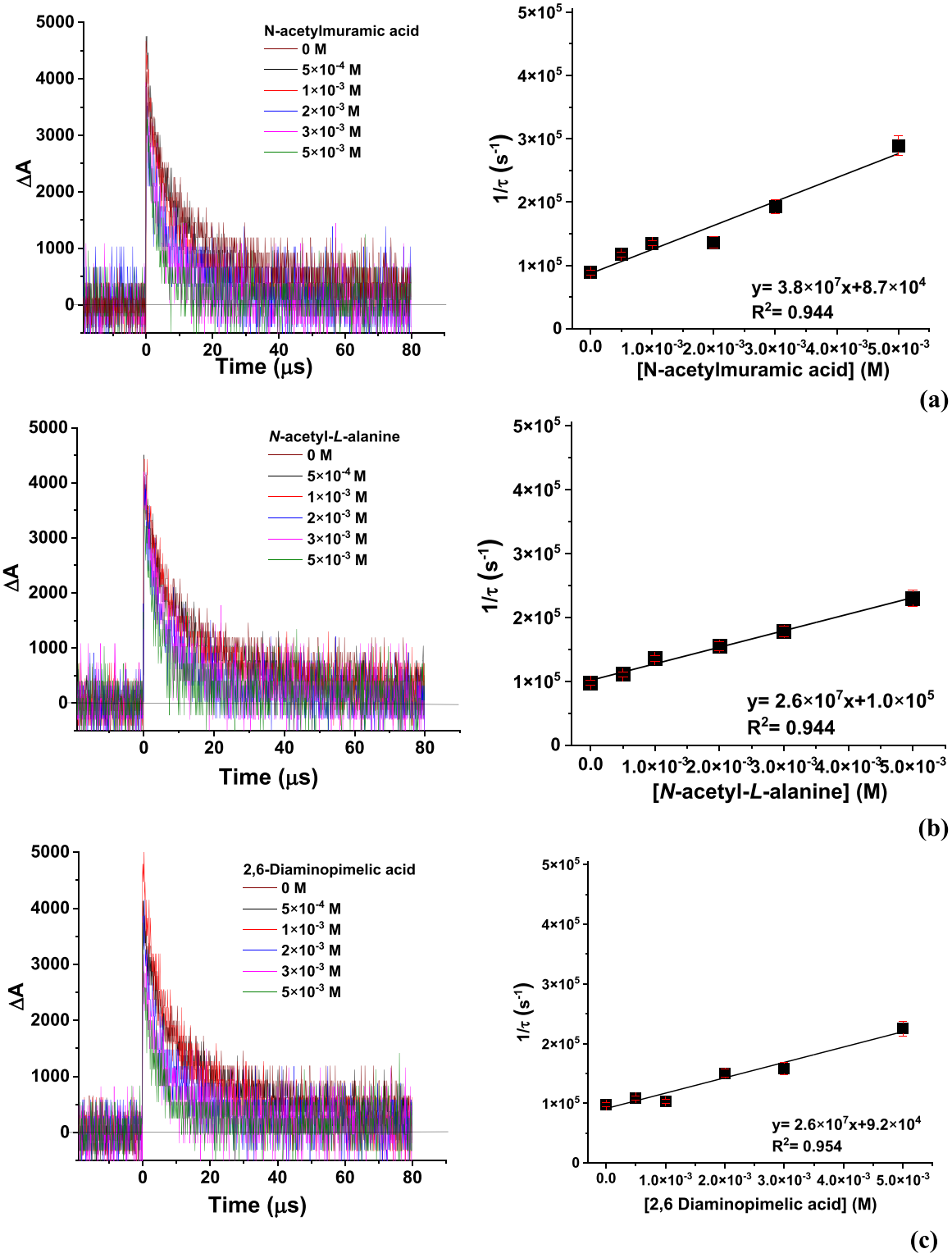

Fig. 2. Left: Decay of $SO_4^{\bullet-}$, monitored at 450 nm, obtained from laser flash excitation (λ_{exc} = 266 nm) of aerated aqueous solutions of PS (0.1 M), in the presence of increasing concentrations of cell-wall constituents: 0 (wine); 5 × 10^{-4} M (black); 1 × 10^{-3} M (red); 2 × 10^{-3} M (blue); 3 × 10^{-3} M (magenta); 5 × 10^{-3} M (olive); *N*-acetylmuramic acid (a); *N*-acetyl-*L*-alanine (b); 2,6-Diaminopimelic acid (c); *N*-acetyl-*D*-glucosamine (d); *N*-acetyl-*L*-lysine (e); *N*-acetyl-*D,L*-glutamic acid (f). Right: corresponding Stern-Volmer plots.

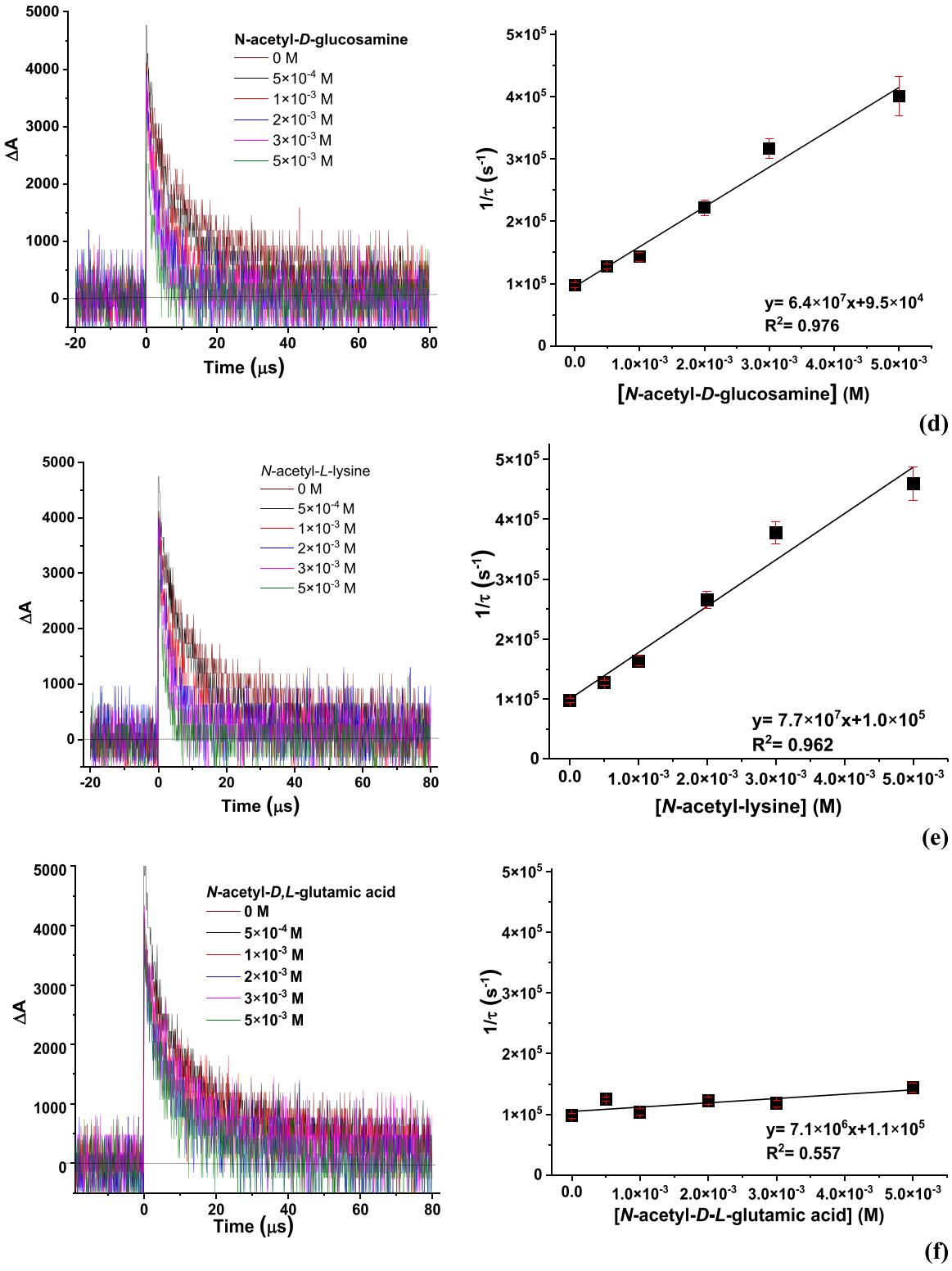

Fig. 2. (*continued*).

3.2. Bacterial inactivation mechanism

3.2.1. Determination of the bimolecular rate constants for the reaction between cell wall constituents and $SO_4^{\bullet-}$

It is well-known that bacterial cell wall is an essential structure that protects cells from mechanical damage and from osmotic rupture or lysis and constitutes an important defense from the attack by different agents. Xiao et al. demonstrated, through SEM imaging of bacteria, that $SO_4^{\bullet-}$ initiates oxidative reactions on the cell wall, with deformation, pore-forming, and fracture of cells [9]. Gram-positive bacteria have a thick peptidoglycan layer; whereas, gram-negative bacteria are characterized by the presence of a thinner membrane surrounded by an outer membrane [27]. Nevertheless, typical constituents of cell wall of both types of bacteria are: *N*-acetylmuramic acid, *N*-acetyl-*L*-alanine, 2,

6-Diaminopimelic acid, *N*-acetyl-*D*-glucosamine, *N*-acetyl-*L*-lysine and *N*-acetyl-*D,L*-glutamic acid (Fig. S1). However, outer membrane proteins (OMPs, mainly porins), which are responsible for the introduction of nutrients inside the cell and the elimination of toxic compound outside, are only present in gram-negative bacteria [28–30]. This type of proteins contains in their primary structure AAA, such as Tryptophan (Trp), Tyrosine (Tyr) and Phenylalanine (Phe), compounds very rich in electrons that can easily be oxidized through electron transfer processes [31–34].

In order to elucidate the mechanisms of the oxidation reactions between $SO_4^{\bullet-}$ and bacteria, $k_{SO4\bullet-}$ for the reaction with the selected biomolecules were measured by LFP. The decay of $SO_4^{\bullet-}$ was monitored at 450 nm in the presence of increasing amounts of all membrane cell constituents commented above (Q) using concentrations ranging from 5×10^{-4} to 5×10^{-3} M. The $k_{SO4\bullet-}$ ($M^{-1}s^{-1}$) values determined from the corresponding Stern-Volmer plots are shown in Fig. 2 and the experimental values are shown in Table 1. The reactivity order of these cell-wall components was: *N*-acetyl-*L*-lysine > *N*-acetyl-*D*-glucosamine > *N*-acetylmuramic acid > 2,6-Diaminopimelic acid ≅ *N*-acetyl-*L*-alanine > *N*-acetyl-*D,L*-glutamic acid. These results reveal that reactivity of all the common biomolecules with $SO_4^{\bullet-}$ is in the range of 7.1×10^6 - 7.1×10^7 $M^{-1}s^{-1}$, in the order to the values obtained with H-donor models (in the range of 10^7 $M^{-1}s^{-1}$, much lower than those that would result from electron-transfer mechanism 10^9 $M^{-1}s^{-1}$). The particular reactivity of each cell-wall component showed similar $k_{SO4\bullet-}$ in all cases, except for *N*-acetyl-*D,L*-glutamic acid that reacted with $SO_4^{\bullet-}$ with one order of magnitude smaller compared with the others.

This result supports the inactivation mechanisms initiated by a H-transfer to $SO_4^{\bullet-}$ involving C-H bond in the cell-wall membrane compounds, generating damages by oxidative stress, eventually leading to bacterial inactivation. Clifton et al. demonstrated the involvement of C-H bond by excluding the O-H bond, since experiments in the presence of methanol deuterated on oxygen or no deuterated one, gave no differences in the rate constants with $SO_4^{\bullet-}$. Moreover, it has been demonstrated that OH and NH_2- group enhanced H-abstraction of α C-H bond [24,35], while an opposite effect of withdrawing electron group (such as –COOH) could cause a decrease of the H transfer efficiency. This effect was also observed in our study for *N*-acetyl-*D,L*-glutamic acid and it could explain the lower kinetic constant value obtained. Previous results in the literature have found that $SO_4^{\bullet-}$ damages and attacks the cell membrane/wall, proteins, and genetic material, resulting in the inactivation of the microorganisms. The destruction of the cell-wall or membrane has been indicated by Scanning Electron Microscope (SEM) images, and it results in perturbed membrane permeability, inhibiting normal metabolism and thus leading to the inactivation of cells. Afterwards, $SO_4^{\bullet-}$ can also permeate through the cell membrane and further reacts with cellular components [36]. It has been also revealed that $SO_4^{\bullet-}$ reacted with high specificity with electron-rich moieties of those surface-bound macromolecules on the surface of *E. coli* O157:H7 cell membrane [37].

Nevertheless, when the reactivity of $SO_4^{\bullet-}$ was studied with the AAA (Tryptophan (Trp), Tyrosine (Tyr) and Phenylalanine (Phe)), the $k_{SO4\bullet-}$ values were two and three orders of magnitude higher than those determined for the common membrane biomolecules (Table 1).

Table 1
Bimolecular rate constants $k_{SO4\bullet-,Q}$ ($M^{-1}s^{-1}$) between $SO_4^{\bullet-}$ and cell-wall constituents.

Cell wall constituents	$k_{SO4\bullet-}$ ($M^{-1}s^{-1}$)
N-acetylmuramic acid	$(3.8 \pm 0.4) \times 10^7$
N-acetyl-*L*-alanine	$(2.6 \pm 0.1) \times 10^7$
2,6-Diaminopimelic acid	$(2.6 \pm 0.3) \times 10^7$
N-acetyl-*D*-glucosamine	$(6.4 \pm 0.4) \times 10^7$
N-acetyl-*L*-lysine	$(7.7 \pm 0.7) \times 10^7$
N-acetyl-*D,L*-glutamic acid	$(7.1 \pm 3.0) \times 10^6$
Tryptophan	$(6.7 \pm 1.0) \times 10^9$
Tyrosine	$(1.0 \pm 0.1) \times 10^9$
Phenylalanine	$(1.4 \pm 0.4) \times 10^9$

Fig. 3a shows the transient absorption spectrum obtained from a deaerated solution of PS (0.1 M) in the presence of Trp (2×10^{-4} M). At short times after the laser pulse, the signal with two maxima (320 and 450 nm, black trace) corresponds to the $SO_4^{\bullet-}$ (Fig. S4). At longer times, a second species arises with two absorption maxima at *ca.* 320 nm and 550 nm, corresponding to the transient absorption spectra of Trp(-H)$^{\bullet}$, in agreement with the literature (Fig. S5a) [32,38]. The quenching rate constant for the reaction between the $SO_4^{\bullet-}$ and Trp, was determined from the growth corresponding to the formation of the Trp(-H)$^{\bullet}$, recorded in a clean region of the available spectral window (550 nm) (Fig. 3b). Thus, the corresponding Stern-Volmer analysis (Fig. 3c) gave a bimolecular rate constant value of $(6.7 \pm 1) \times 10^9$ $M^{-1}s^{-1}$ (Table 1).

In the case of Tyr, transient absorption spectrum show the characteristic of Tyr(-H)$^{\bullet}$ (Fig. S5b) after the complete disappearance of $SO_4^{\bullet-}$ (Fig. 4a); the decrease in the lifetime of $SO_4^{\bullet-}$ and the corresponding Stern-Volmer plot are shown in Fig. 4b and c, respectively.

Analogously, increasing concentrations of the aromatic Phe produced a decrease in the lifetime of $SO_4^{\bullet-}$ with a bimolecular rate constant value of $(1.4 \pm 0.4) \times 10^9$ $M^{-1}s^{-1}$ (Fig. S6a and b and Table 1). The resulting transient absorption spectrum showed a new band peaking at *ca.* 300 nm that could not be unambiguously assigned on the basis of the available literature data and was not further investigated [38].

The direct observation of oxidized radicals of Trp and Tyr has provided unambiguous evidence for the electron transfer process. In fact, considering Trp and Tyr, electron transfer from Trp or Tyr to the oxidant led to the formation of Trp$^{\bullet+}$ or Tyr$^{\bullet+}$, that subsequently deprotonate to yield the much longer-lived radicals Trp(-H)$^{\bullet}$ or Tyr(-H)$^{\bullet}$, as a result of a global proton coupled electron transfer mechanism (PCTE) and as it is shown in Fig. S5 [32]. Moreover, these values are in agreement with typical values corresponding to an electron transfer mechanism (see above). In the case of Phe, an electron transfer to the $SO_4^{\bullet-}$ seems also to occur, but on the basis of the determined rate constant value we cannot discard the possibility that an addition of $SO_4^{\bullet}$ to its aromatic ring could have been taken place [8].

With this scenario, a difference in the bacteria inactivation reactivity could be envisaged, because all the membrane components (at least the predominant molecules) of gram-positive bacteria present a low reactivity with $SO_4^{\bullet-}$ in agreement with a H-abstraction mechanism; whereas in the case of the gram-negative bacteria, there are key biomolecules (proteins such as porins) in their membranes that contain AAA highly reactive against $SO_4^{\bullet-}$, through electron transfer mechanisms (Fig. 5).

3.2.2. Bacterial inactivation kinetics by sulfate radical anion

The macromolecular reactivity of $SO_4^{\bullet-}$ against bacteria was assessed at pilot plant scale by exposure to UV-C radiation, a well-known activation method of PS in water. Prior to that, dark control tests, with and without oxidant, were performed to estimate any potential PS bactericidal and/or osmotic stress effect on bacterial viability (Fig. S7a). Results showed that in the absence of PS, no loss of viability (initial concentration *ca.* 10^6 CFU/mL) was observed for *E. coli* and *E. faecalis* after 30 min. By adding PS, at an initial concentration of 5×10^{-4} M, a significant oxidative effect of PS by itself was not observed; 0.7 logarithmic reduction value (LRV) was achieved after 30 min for *E. coli*, while no loss of viability was observed for *E. faecalis*. This behaviour has also been confirmed by other authors in literature. Rodríguez-chueca et al. and Ferreira et al. reported no bactericidal effect in dark conditions for PS at concentrations of 1.8×10^{-5} – 9×10^{-5} M and 7×10^{-4} M, respectively [39,40].

The solely effect of UV-C radiation over each bacterium was also assessed, due to its well-known capacity for microbial abatement in water [41]. Then, different concentrations of PS were tested in order to determine the bacterial kinetics by SR-AOP in the presence of PS as a source of $SO_4^{\bullet-}$. Fig. S7b and c show double log linear fitting of *E. coli* and *E. faecalis* under UV-C light, respectively.

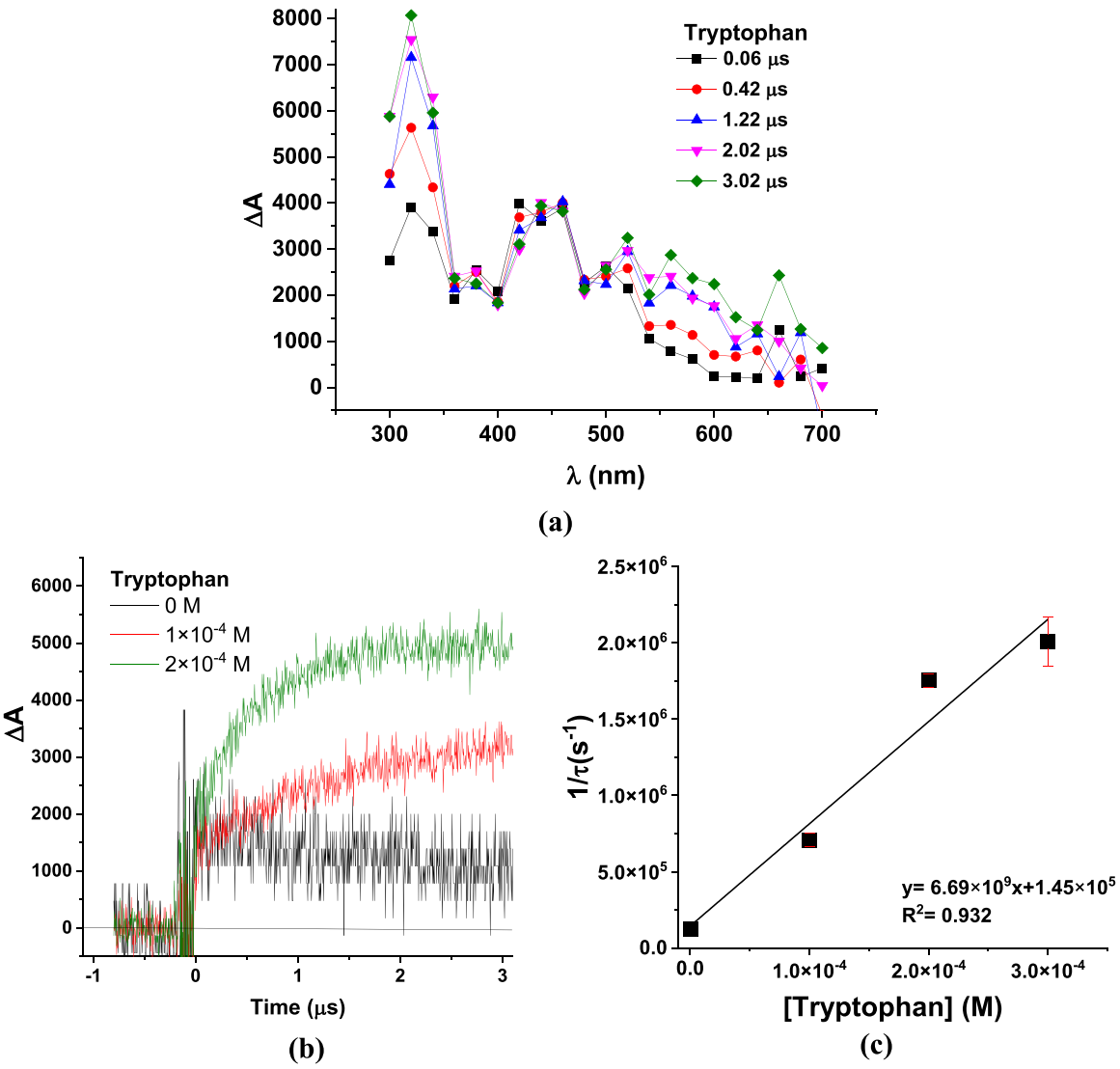

Fig. 3. Transient absorption spectra obtained from aerated aqueous solutions of PS (0.1 M) in the presence of Trp (2×10^{-4} M), recorded at different times after the laser pulse ($\lambda_{exc} = 266$ nm): 0.06 µs (black); 0.42 µs (red); 1.22 µs (blue); 2.02 µs (magenta); 3.02 µs (green) (a). Transient absorption traces monitored at 550 nm, obtained upon laser pulse ($\lambda_{exc} = 266$ nm) from an aerated aqueous solution of PS (0.1 M) in the presence of different concentrations of Trp: 0 (black); 1×10^{-4} M (red) and 2×10^{-4} M (green) (b). Corresponding Stern-Volmer plot (c).

In the presence of 1.3×10^{-4} M PS concentration, no significant differences were observed between inactivation kinetic constants in the presence and in the absence of oxidant for each bacterium, while an increase of PS dosage from 3×10^{-4} to 5×10^{-4} M led to an enhancement in bacterial inactivation, comparing to only UV-C treatment.

The pseudo-first order kinetic constants obtained from the second stage (k_2) of both bacteria, were plotted as a function of PS concentration and a linear relationship was found, as it can be observed in Fig. 6. The following kinetic constants were calculated, highlighting this reactivity order: $k_{E.\ coli,\ PS}$ (1003 ± 108) $M^{-1}\ min^{-1} > k_{E.\ faecalis,\ PS}$ (892 ± 101) $M^{-1}\ min^{-1}$. Higher susceptibility of gram-negative bacteria to the water treatment compared to gram-positive was clearly determined. This difference could be correlated with the LFP results and the envisaged mechanisms previously described. Thus, AAA of the porins of the gram-negative outer-membrane react with $SO_4^{\bullet-}$ thought electron transfer processes which may result in a fast denaturalization of the protein and consequently an alteration of the outer-membrane permeability. Therefore, the presence of AAA on the cell-wall of gram-negative bacteria could be a reasonable explanation of the higher inactivation of *E. coli* in comparison with *E. faecalis* (gram-positive bacteria) because the common cell-wall components present in both types of bacteria cell-wall react through H-abstraction mechanism.

In this context, previous studies showed different resistance of gram-negative and gram-positive bacteria to disinfectants but although most of them have reported that gram-positive bacteria are more resistant than gram-negative bacteria, opposite has been also reported. Nevertheless, all of them have attributed these differences mainly to the different physiological structures and chemical compositions of the cell walls [42–47]. However, reactivity of the components of the bacteria wall with the oxidant species generated from the disinfectant has not been reported. Now, the data obtained herein provide evidence to understand the rate of the initial oxidation processes for the bacteria inactivation caused by $SO_4^{\bullet-}$.

3.3. Degradation mechanism for the Contaminants of Emerging Concern (CECs)

3.3.1. Determination of the bimolecular rate constants between $SO_4^{\bullet-}$ and CECs by LFP

The reactivity between $SO_4^{\bullet-}$ and the selected CECs (DCF, SMX and

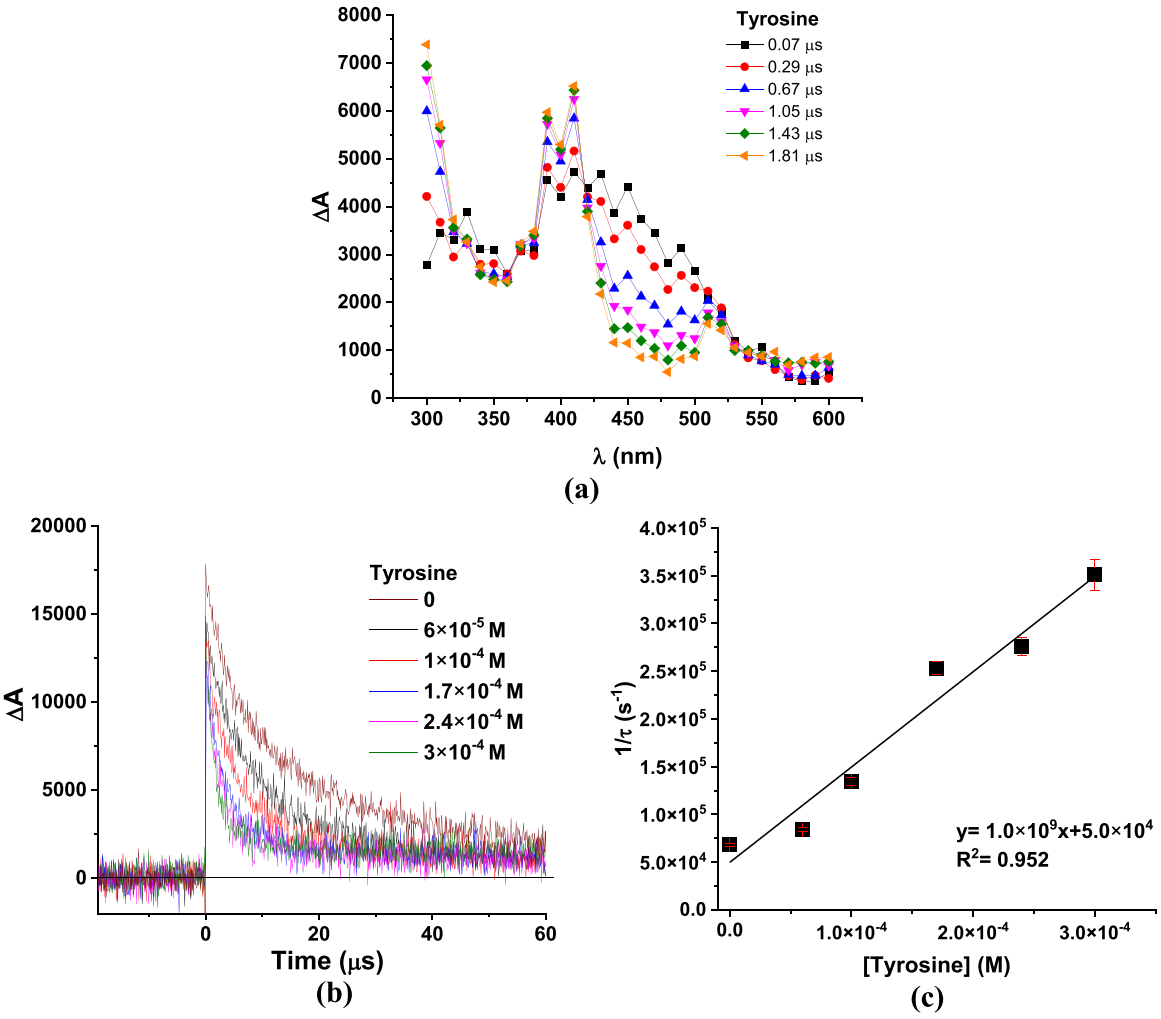

Fig. 4. Transient absorption spectra obtained from aerated aqueous solutions of PS (0.1 M) in the presence of Tyr (3×10^{-4} M), recorded at different times after the laser pulse ($\lambda_{exc} = 266$ nm): 0.07 µs (black); 0. 29 µs (red); 0.67 µs (blue); 1.05 µs (magenta); 1.43 µs (olive); 1.81 µs (orange) (a). Decay of $SO_4^{\bullet-}$, obtained from laser flash excitation ($\lambda_{exc} = 266$ nm) of aerated solutions of PS (0.1 M), monitored at 450 nm, in the presence of increasing concentrations of Tyr: 0 (wine); 6×10^{-5} M (black); 1×10^{-4} M (red); 1.7×10^{-4} M (blue); 2.4×10^{-4} M (magenta); 3×10^{-4} M (olive) (b). Corresponding Stern-Volmer plot (c).

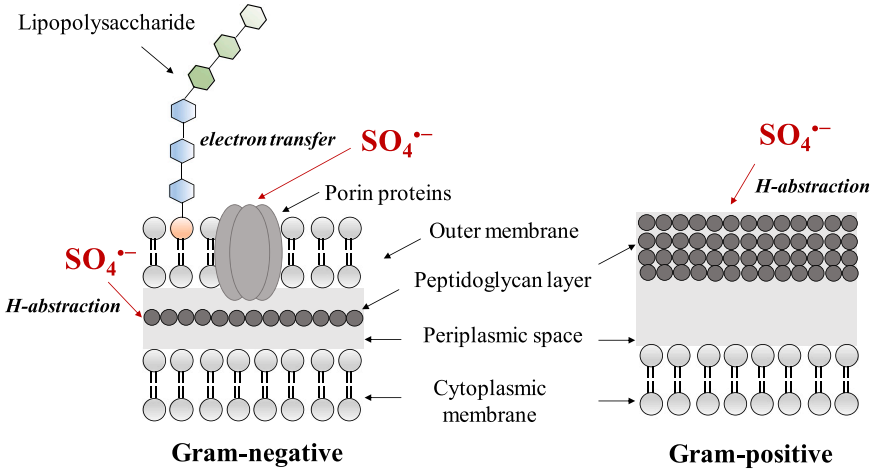

Fig. 5. Schematic representation of cell-wall of gram-negative and gram-positive bacteria.

TMP), chosen due to their intensive use, low biodegradability, chemical stability and incomplete removal in urban wastewater treatment plants (UWWTPs), was assessed on the basis of LFP experiments. In this context, as CECs are also excited at the excitation wavelength of 266 nm, aqueous solution of DCF, SMX and TMP at 2×10^{-4} M in aerobic media were initially studied upon LFP irradiation in order to detect the possible

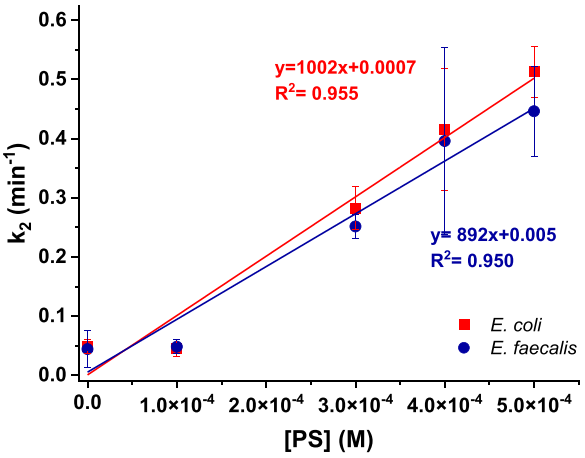

Fig. 6. Second stage bacterial inactivation pseudo-first order kinetic constant k_2 as a function of PS concentration (M) for *E. coli* (■) and *E. faecalis* (●) under UV-C irradiation.

formation of some transient species absorbing around 450 nm (Fig. S8). Fortunately, no intermediate was observed for the CECs. Thereby, quenching experiments performed using the decay of $SO_4^{\bullet-}$ at 450 nm could be associated only to the generated radical anion species.

Fig. S9 shows the decays of $SO_4^{\bullet-}$, monitored at 450 nm, in the presence of different concentrations of DCF, SMX and TMP ($0 - 5 \times 10^{-5}$ M). The slope of Stern-Volmer plots provided $k_{SO4\bullet-}$ with the following reactivity order: DCF ($(2.2 \pm 0.2) \times 10^9$ $M^{-1}s^{-1}$) > TMP ($(1.4 \pm 0.1) \times 10^9$ $M^{-1}s^{-1}$) ≅ SMX ($(1.2 \pm 0.2) \times 10^9$ $M^{-1}s^{-1}$). These experimental values agree with literature data, and they are near-diffusion-controlled reactions, in the order of the kinetic constants obtained upon electron transfer mechanism (reaction rates in the order of 10^9 $M^{-1}s^{-1}$) [5,17].

Interestingly, although Mahdi Ahmed et al. determined, by using competition kinetics technique, too high values for the $k_{SO4\bullet-}$ with DCF and SMX ($(12.5 \pm 3.1) \times 10^9$ and $(9.2 \pm 2.6) \times 10^9$ M^{-1} s^{-1}, respectively), they obtained the same reactivity order than that determined in the present study. Moreover, they postulated that the formation of an *N*-centred radical, through probably a one-electron transfer mechanism, was the starting point of the degradation pathway of both compounds [48]. However, on the basis of the results obtained here with CECs, it is not possible to discard that the observed reactivity was partially produced by the addition of $SO_4^{\bullet-}$ to a double bond of the selected CECs.

3.3.2. CECs degradation by sulfate radical anion

As for bacteria, the degradation kinetic of each CEC by SR-AOP, using PS as source of sulfate radicals and UV-C as activation method, has been investigated in order to translate LFP results to a real water decontamination removal process at pilot plant scale.

Control experiments under dark conditions revealed that SMX and TMP were not degraded after 30 min, while 66% of DCF was removed in the presence of 5×10^{-4} M of PS (Fig. S10a). Comparative degradation profiles of DCF, SMX and TMP in the absence and in the presence of increasing concentrations of PS under UV-C radiation at pilot plant scale are shown in Fig. S10b, c and d, respectively. UV direct photolysis was an important contribution in DCF and SMX removal with pseudo-first order degradation kinetic constants of (0.35 ± 0.03) min^{-1} and (0.39 ± 0.04) min^{-1}, respectively, while negligible TMP degradation was observed under only UV irradiation. Nevertheless, the process was enhanced by adding increasing concentration of PS and linear relationship between pseudo first order degradation constants and PS dosage was obtained (Fig. 7). The following reactivity order was found: DCF (3983 ± 376) M^{-1} min^{-1} > SMX (1215 ± 190) M^{-1} min^{-1} > TMP (878 ± 165) M^{-1} min^{-1}, highlighting higher reactivity of DCF, compared to SMX and TMP, in good agreement with $k_{SO4\bullet-}$, values obtained with LFP experiments.

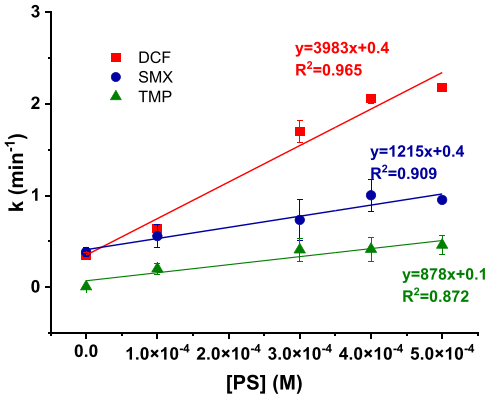

Fig. 7. Pseudo-first order kinetic constant as a function of PS concentration (M) for DCF (■), SMX (●) and TMP (▲) under UV-C radiation.

Besides, the role of $HO^{\bullet}$ in CECs degradation has been evaluated, conducting experiments with and without TBA, capable of reacting with higher efficiency with $HO^{\bullet}$ than $SO_4^{\bullet-}$ [49]. Similar degradation profiles were obtained for each CEC in the presence and in the absence of the quenching agent (Fig. S11), highlighting that $SO_4^{\bullet-}$ was the predominant radical, while $HO^{\bullet}$ was not the responsible for CECs removal under these experimental conditions, as it has been also outlined in previous works [49,50].

3.4. Simultaneous disinfection and decontamination: validation of the targets reactivity order

Afterwards, the effect of the simultaneous present of all targets on process performance was evaluated and compared to each individual system (chemical or biological) and the results in the presence of a concentration of PS of 5×10^{-5} M are shown in Figs. S7 and S10 and Table 1. The same reactivity order previously found was obtained, highlighting its independence from competitiveness between targets pollutants. However, it could be observed that CECs degradation was not significant affected by the presence of bacteria, while ≈ 2 times lower inactivation kinetic constants were obtained for both bacteria. This difference could be attributed to the different physical phases between bacteria (suspended particles) and CECs (dissolved organic compound). CECs could react more rapid with radical species in solution than bacteria, obtaining only a detrimental effect of their presence on pathogens inactivation, but no vice versa. Moreover, it has been found in a previous study that the reactivity order was independent also from other potential naturally occurring contaminants such as organic matter and inorganic chemical, evaluating the simultaneous removal of the same chemical and microbial targets, in the presence of PMS ($0.01–1 \times 10^{-3}$ M) and UV-C radiation in simulated and actual urban wastewater [51]. Another application of SR-AOPs both for the inactivation of microorganisms (*E. coli* and *E. faecalis*) and for the removal of CECs in real wastewater treatment plant effluents showed that *E. faecalis* was more resistant than *E. coli,* supporting the mechanistic study conducted in the present work and confirming the bacteria reactivity order found against $SO_4^{\bullet-}$ [52].

4. Conclusions

The reactivity of $SO_4^{\bullet-}$ against gram-negative (*E. coli*) and gram-positive (*E. faecalis*) bacteria and CECs (Diclofenac-DCF, Sulfamethoxazole-SMX and Trimethoprim-TMP) was investigated through laser flash photolysis technique. Analysis of the lifetime of $SO_4^{\bullet-}$ in presence of typical constituents of cell-wall of bacteria and CECs allowed determining reactivity of $SO_4^{\bullet-}$ towards these compounds. Results showed that $SO_4^{\bullet-}$ reacts with common cell-wall components present in gram-negative bacteria strain and in gram-positive ones through H-abstraction mechanism ($k_{SO4\bullet-} < 10^8$ $M^{-1}s^{-1}$). In addition, $k_{SO4\bullet-}$ >

10^9 $M^{-1}s^{-1}$ were found using aromatic amino acids contained in the skeleton of porins, proteins of out-sphere membrane of gram-negative bacteria. Detection of the resulting intermediates confirmed the electron transfer mechanism operating in such cases. Besides, $k_{SO4\bullet-}$ values determined for DCF, TMP and SMX are compatible with electron transfer mechanism.

Moreover, the experiments at pilot plant scale by UV-C/$SO_4^{\bullet-}$ confirmed radical sulfate reactivity towards the bacteria and the three contaminants and demonstrated the potential applicability of SR-AOPs system in water disinfection and decontamination. The following reactivity order was found: *E. coli* > *E. faecalis* and DCF > TMP ≅ SMX, which is fully in accordance with the $k_{SO4\bullet-}$ values determined using LFP technique. Therefore, it has been proven that the rate of the initial reactions of $SO_4^{\bullet-}$ with cell-wall components of bacteria can explain the different resistance of bacteria to inactivation. Even more, the present study has showed the usefulness of time-resolved techniques to investigate on water disinfection and decontamination by $SO_4^{\bullet-}$ in the presence of UV-C irradiation.

CRediT authorship contribution statement

Ilaria Berruti: Investigation, Methodology, Formal analysis, Writing – original draft. **Jenny Flores:** Investigation, Methodology. **Isabel Oller**: Project administration, Writing – review & editing. **Francisco Bosca:** Supervision, Writing – review & editing. **M. Luisa Marin**: Conceptualization, Supervision, Writing – review & editing. **María Inmaculada Polo-López**: Conceptualization, Supervision, Writing – review & editing.

Declaration of Competing Interest

The authors declare that they have no known competing financial interests or personal relationships that could have appeared to influence the work reported in this paper.

Acknowledgments

This work is part of a project that has received funding from the European Union's Horizon 2020 research and innovation programme under the Marie Skłodowska-Curie Grant Agreement No 765860 (AQUAlity). Authors also acknowledge the Spanish Ministry of Science and Innovation (Projects PID2019–110441RB-C32 and PID2019–110441RB-C33). PhD Scholarship from CONACYT for J. Flores-Garcia (709358) is acknowledged.

Appendix A. Supporting information

Supplementary data associated with this article can be found in the online version at doi:10.1016/j.apcatb.2022.121519.

References

[1] X. Xia, F. Zhu, J. Li, H. Yang, L. Wei, Q. Li, J. Jiang, G. Zhang, Q. Zhao, A review study on sulfate-radical-based advanced oxidation processes for domestic/industrial wastewater treatment: degradation, efficiency, and mechanism, Front. Chem. 8 (2020), https://doi.org/10.3389/fchem.2020.592056.

[2] S. Guerra-Rodríguez, E. Rodríguez, D.N. Singh, J. Rodríguez-Chueca, Assessment of sulfate radical-based advanced oxidation processes for water and wastewater treatment: a review, Water (Switz.) 10 (2018), https://doi.org/10.3390/w10121828.

[3] S. Wacławek, H.V. Lutze, K. Grübel, V.V.T. Padil, M. Černík, D.D. Dionysiou, Chemistry of persulfates in water and wastewater treatment: a review, Chem. Eng. J. 330 (2017) 44–62, https://doi.org/10.1016/j.cej.2017.07.132.

[4] R.E. Huie, C.L. Clifton, P. Neta, Electron transfer reaction rates and equilibria of the carbonate and sulfate radical anions, Int. J. Radiat. Appl. Instrum. Part 38 (1991) 477–481, https://doi.org/10.1016/1359-0197(91)90065-A.

[5] L. Wojnárovits, E. Takács, Rate constants of sulfate radical anion reactions with organic molecules: a review, Chemosphere 220 (2019) 1014–1032, https://doi.org/10.1016/j.chemosphere.2018.12.156.

[6] L. Gao, Q. Mao, S. Luo, L. Cao, X. Xie, Y. Yang, Y. Deng, Z. Wei, Experimental and theoretical insights into kinetics and mechanisms of hydroxyl and sulfate radicals-mediated degradation of sulfamethoxazole: similarities and differences, Environ. Pollut. 259 (2020), 113795, https://doi.org/10.1016/j.envpol.2019.113795.

[7] S. Luo, Z. Wei, D.D. Dionysiou, R. Spinney, W.P. Hu, L. Chai, Z. Yang, T. Ye, R. Xiao, Mechanistic insight into reactivity of sulfate radical with aromatic contaminants through single-electron transfer pathway, Chem. Eng. J. 327 (2017) 1056–1065, https://doi.org/10.1016/j.cej.2017.06.179.

[8] R. Xiao, L. Gao, Z. Wei, R. Spinney, S. Luo, D. Wang, D.D. Dionysiou, C.J. Tang, W. Yang, Mechanistic insight into degradation of endocrine disrupting chemical by hydroxyl radical: an experimental and theoretical approach, Environ. Pollut. 231 (2017) 1446–1452, https://doi.org/10.1016/j.envpol.2017.09.006.

[9] R. Xiao, L. Bai, K. Liu, Y. Shi, D. Minakata, C.H. Huang, R. Spinney, R. Seth, D. D. Dionysiou, Z. Wei, P. Sun, Elucidating sulfate radical-mediated disinfection profiles and mechanisms of *Escherichia coli* and *Enterococcus faecalis* in municipal wastewater, Water Res. 173 (2020), 115552, https://doi.org/10.1016/j.watres.2020.115552.

[10] J. Rodríguez-Chueca, T. Silva, J.R. Fernandes, M.S. Lucas, G.L. Puma, J.A. Peres, A. Sampaio, Inactivation of pathogenic microorganisms in freshwater using HSO_5^-/UV-A LED and HSO_5^-/Mn^+/UV-A LED oxidation processes, Water Res. 123 (2017) 113–123, https://doi.org/10.1016/j.watres.2017.06.021.

[11] D. Xia, Y. Li, G. Huang, R. Yin, T. An, G. Li, H. Zhao, A. Lu, P.K. Wong, Activation of persulfates by natural magnetic pyrrhotite for water disinfection: efficiency, mechanisms, and stability, Water Res. 112 (2017) 236–247, https://doi.org/10.1016/j.watres.2017.01.052.

[12] D. Xia, H. He, H. Liu, Y. Wang, Q. Zhang, Y. Li, A. Lu, C. He, P.K. Wong, Persulfate-mediated catalytic and photocatalytic bacterial inactivation by magnetic natural ilmenite, Appl. Catal. B Environ. 238 (2018) 70–81, https://doi.org/10.1016/j.apcatb.2018.07.003.

[13] S.P. Pitre, C.D. McTiernan, J.C. Scaiano, Understanding the kinetics and spectroscopy of photoredox catalysis and transition-metal-free alternatives, Acc. Chem. Res. 49 (2016) 1320–1330, https://doi.org/10.1021/acs.accounts.6b00012.

[14] M.L. Dell'Arciprete, C.J. Cobos, D.O. Mártire, J.P. Furlong, M.C. Gonzalez, Reaction kinetics and mechanisms of neonicotinoid pesticides with sulfate radicals, N. J. Chem. 35 (2011) 672–680, https://doi.org/10.1039/c0nj00726a.

[15] J.A. Khan, X. He, N.S. Shah, H.M. Khan, E. Hapeshi, D. Fatta-Kassinos, D. D. Dionysiou, Kinetic and mechanism investigation on the photochemical degradation of atrazine with activated H_2O_2, $S_2O_8^{2-}$ and HSO_5^-, Chem. Eng. J. 252 (2014) 393–403, https://doi.org/10.1016/j.cej.2014.04.104.

[16] D.F. Mercado, L.L.B. Bracco, A. Arques, M.C. Gonzalez, P. Caregnato, Reaction kinetics and mechanisms of organosilicon fungicide flusilazole with sulfate and hydroxyl radicals, Chemosphere 190 (2018) 327–336, https://doi.org/10.1016/j.chemosphere.2017.09.134.

[17] Y. Wu, Y. Shi, H. Chen, J. Zhao, W. Dong, Activation of persulfate by magnetite: implications for the degradation of low concentration sulfamethoxazole, Process Saf. Environ. Prot. (2018), https://doi.org/10.1016/j.psep.2018.03.020.

[18] I. Sánchez-Montes, I. Salmerón García, G. Rivas Ibañez, J.M. Aquino, M.I. Polo-López, S. Malato, I. Oller, UVC-based advanced oxidation processes for simultaneous removal of microcontaminants and pathogens from simulated municipal wastewater at pilot plant scale, Environ. Sci. Water Res. Technol. (2020), https://doi.org/10.1039/d0ew00279h.

[19] J. Wang, S. Wang, Activation of persulfate (PS) and peroxymonosulfate (PMS) and application for the degradation of emerging contaminants, Chem. Eng. J. 334 (2018) 1502–1517, https://doi.org/10.1016/j.cej.2017.11.059.

[20] I. Berruti, I. Oller, M.I. Polo-Lopez, Direct oxidation of peroxymonosulfate under natural solar radiation: accelerating the simultaneous removal of organic contaminants and pathogens from water, Chemosphere 279 (2021), https://doi.org/10.1016/j.chemosphere.2021.130555.

[21] I. García-Fernández, S. Miralles-Cuevas, I. Oller, S. Malato, P. Fernández-Ibáñez, M. I. Polo-López, Inactivation of *E. coli* and *E. faecalis* by solar photo-Fenton with EDDS complex at neutral pH in municipal wastewater effluents, J. Hazard. Mater. 372 (2019) 85–93, https://doi.org/10.1016/j.jhazmat.2018.07.037.

[22] K.L. Ivanov, E.M. Glebov, V.F. Plyusnin, Y.V. Ivanov, V.P. Grivin, N.M. Bazhin, Laser flash photolysis of sodium persulfate in aqueous solution with additions of dimethylformamide, J. Photochem. Photobiol. A Chem. 133 (2000) 99–104, https://doi.org/10.1016/S1010-6030(00)00218-5.

[23] Y. Wu, A. Bianco, M. Brigante, W. Dong, P. De Sainte-Claire, K. Hanna, G. Mailhot, Sulfate radical photogeneration using Fe-EDDS: influence of critical parameters and naturally occurring scavengers, Environ. Sci. Technol. 49 (2015) 14343–14349, https://doi.org/10.1021/acs.est.5b03316.

[24] C.L. Clifton, R.E. Huie, Rate constants for hydrogen abstraction reactions of the sulfate radical, SO_{4-} alcohols, Int. J. Chem. Kinet. 21 (1989) 677–687, https://doi.org/10.1002/kin.550210807.

[25] B. Zeev, The redox potential of the azide / azldyl couple, J. Phys. Chem. 91 (1987) 2120–2122, https://doi.org/10.1021/j100292a029.

[26] R.E. Huie, J.T. Herron, Temperature dependence of the rate constants for reactions of ozone with some olefins, J. Phys. Chem. 94 (1990) 8561–8567, https://doi.org/10.1021/j100386a015.

[27] S. Galdiero, A. Falanga, M. Cantisani, R. Tarallo, M. Elena Della Pepa, V. D'Oriano, M. Galdiero, Microbe-host interactions: structure and role of gram-negative bacterial porins, Curr. Protein Pept. Sci. 13 (2012) 843–854, https://doi.org/10.2174/138920312804871120.

[28] A.J. De Jesus, T.W. Allen, The role of tryptophan side chains in membrane protein anchoring and hydrophobic mismatch, Biochim. Biophys. Acta - Biomembr. 1828 (2013) 864–876, https://doi.org/10.1016/j.bbamem.2012.09.009.

[29] K.M. Sanchez, G. Kang, B. Wu, J.E. Kim, Tryptophan-lipid interactions in membrane protein folding probed by ultraviolet resonance Raman and fluorescence spectroscopy, Biophys. J. 100 (2011) 2121–2130, https://doi.org/10.1016/j.bpj.2011.03.018.
[30] A.H. O'Keeffe, J.M. East, A.G. Lee, Selectivity in lipid binding to the bacterial outer membrane protein OmpF, Biophys. J. 79 (2000) 2066–2074, https://doi.org/10.1016/S0006-3495(00)76454-X.
[31] G. Bosio, S. Criado, W. Massad, F.J. Rodríguez Nieto, M.C. Gonzalez, N.A. García, D.O. Mártire, Kinetics of the interaction of sulfate and hydrogen phosphate radicals with small peptides of glycine, alanine, tyrosine and tryptophan, Photochem. Photobiol. Sci. 4 (2005) 840–846, https://doi.org/10.1039/b507856c.
[32] R.I. Teixeira, J.S. Goulart, R.J. Corrêa, S.J. Garden, S.B. Ferreira, J.C. Netto-Ferreira, V.F. Ferreira, P. Miro, M.L. Marin, M.A. Miranda, N.C. De Lucas, A photochemical and theoretical study of the triplet reactivity of furano- and pyrano-1,4-naphthoquinonones towards tyrosine and tryptophan derivatives, RSC Adv. 9 (2019) 13386–13397, https://doi.org/10.1039/c9ra01939a.
[33] A. Harriman, Further comments on the redox potentials of tryptophan and tyrosine, J. Phys. Chem. 91 (1987) 6102–6104, https://doi.org/10.1021/j100308a011.
[34] D.M. Close, P. Wardman, Calculation of standard reduction potentials of amino acid radicals and the effects of water and incorporation into peptides, J. Phys. Chem. A. 122 (2018) 439–445, https://doi.org/10.1021/acs.jpca.7b10766.
[35] I. MacInnes, J.C. Walton, D.C. Nonhebel, Hydrogen abstraction from primary amines. substituent effects on the carbon-nitrogen bond rotation barriers in aminoalkyl radicals, J. Chem. Soc. Perkin Trans. 2 (1987) 1789–1794, https://doi.org/10.1039/p29870001789.
[36] R. Xiao, K. Liu, L. Bai, D. Minakata, Y. Seo, R. Kaya Göktaş, D.D. Dionysiou, C. J. Tang, Z. Wei, R. Spinney, Inactivation of pathogenic microorganisms by sulfate radical: present and future, Chem. Eng. J. 371 (2019) 222–232, https://doi.org/10.1016/j.cej.2019.03.296.
[37] D.N. Wordofa, S.L. Walker, H. Liu, Sulfate radical-induced disinfection of pathogenic *Escherichia coli* O157:H7 via iron-activated persulfate, Environ. Sci. Technol. Lett. 4 (2017) 154–160, https://doi.org/10.1021/acs.estlett.7b00035.
[38] R.V. Bensasson E.J. Land T.G. Truscott Flash Photolysis and Pulse Radiolysis: Contributions to the Chemistry of Biology and Medicine 1983 236.
[39] J. Rodríguez-chueca, S. Giannakis, M. Marjanovic, M. Kohantorabi, M. Reza, D. Grandjean, L. Felippe, D. Alencastro, Solar-assisted bacterial disinfection and removal of contaminants of emerging concern by Fe^{2+} -activated HSO_5^- vs. $S_2O_8^{2-}$ in drinking water, Appl. Catal. B Environ. 248 (2019) 62–72, https://doi.org/10.1016/j.apcatb.2019.02.018.
[40] L.C. Ferreira, M. Castro-Alférez, S. Nahim-Granados, M.I. Polo-López, M.S. Lucas, G. Li Puma, P. Fernández-Ibáñez, Inactivation of water pathogens with solar photo-activated persulfate oxidation, Chem. Eng. J. 381 (2020), 122275, https://doi.org/10.1016/j.cej.2019.122275.
[41] J. Rodríguez-Chueca, C. García-Cañibano, R.J. Lepistö, J. Encinas, J. Pellinen, Marugán, Intensification of UV-C tertiary treatment: disinfection and removal of micropollutants by sulfate radical based advanced oxidation processes, J. Hazard. Mater. (2019) 94–102, https://doi.org/10.1016/j.jhazmat.2018.04.044.
[42] E. Bae, J.W. Lee, B.H. Hwang, J. Yeo, J. Yoon, H.J. Cha, W. Choi, Photocatalytic bacterial inactivation by polyoxometalates, Chemosphere 72 (2008) 174–181, https://doi.org/10.1016/j.chemosphere.2008.01.071.
[43] K.P. Kühn, I.F. Chaberny, K. Massholder, M. Stickler, V.W. Benz, H.G. Sonntag, L. Erdinger, Disinfection of surfaces by photocatalytic oxidation with titanium dioxide and UVA light, Chemosphere 53 (2003) 71–77, https://doi.org/10.1016/S0045-6535(03)00362-X.
[44] O. Seven, B. Dindar, S. Aydemir, D. Metin, M.A. Ozinel, S. Icli, Solar photocalytic disinfection of a group of bacteria and fungi aqueous suspensions with TiO_2, ZnO and sahara desert dust, J. Photochem. Photobiol. A Chem. 165 (2004) 103–107, https://doi.org/10.1016/j.jphotochem.2004.03.005.
[45] R. van Grieken, J. Marugán, C. Pablos, L. Furones, A. López, Comparison between the photocatalytic inactivation of Gram-positive *E. faecalis* and Gram-negative *E. coli* faecal contamination indicator microorganisms, Appl. Catal. B Environ. 100 (2010) 212–220, https://doi.org/10.1016/j.apcatb.2010.07.034.
[46] A.I. Gomes, V.J.P. Vilar, R.A.R. Boaventura, Synthetic and natural waters disinfection using natural solar radiation in a pilot plant with CPCs, Catal. Today 144 (2009) 55–61, https://doi.org/10.1016/j.cattod.2008.12.023.
[47] T.N. Demidova, M.R. Hamblin, Effect of cell-photosensitizer binding and cell density on microbial photoinactivation, Antimicrob. Agents Chemother. 49 (2005) 2329–2335, https://doi.org/10.1128/AAC.49.6.2329-2335.2005.
[48] M. Mahdi Ahmed, S. Barbati, P. Doumenq, S. Chiron, Sulfate radical anion oxidation of diclofenac and sulfamethoxazole for water decontamination, Chem. Eng. J. 197 (2012) 440–447, https://doi.org/10.1016/j.cej.2012.05.040.
[49] E.A. Serna-Galvis, F. Ferraro, J. Silva-Agredo, R.A. Torres-Palma, Degradation of highly consumed fluoroquinolones, penicillins and cephalosporins in distilled water and simulated hospital wastewater by UV254 and UV254/persulfate processes, Water Res. 122 (2017) 128–138, https://doi.org/10.1016/j.watres.2017.05.065.
[50] C.C. Lin, M.S. Wu, Degradation of ciprofloxacin by UV/$S_2O_8^{2-}$ process in a large photoreactor, J. Photochem. Photobiol. A Chem. 285 (2014) 1–6, https://doi.org/10.1016/j.jphotochem.2014.04.002.
[51] I. Berruti, S. Nahim-Granados, M.J. Abeledo-Lameiro, I. Oller, M.I. Polo-López, UV-C peroxymonosulfate activation for wastewater regeneration: Simultaneous inactivation of pathogens and degradation of contaminants of emerging concern, Molecules 26 (2021), https://doi.org/10.3390/molecules26164890.
[52] J. Rodríguez-Chueca, C. García-Cañibano, R.J. Lepistö, J. Encinas, J. Pellinen, Marugán, Intensification of UV-C tertiary treatment: disinfection and removal of micropollutants by sulfate radical based advanced oxidation processes, J. Hazard. Mater. 372 (2019) 94–102, https://doi.org/10.1016/j.jhazmat.2018.04.044.